IJICTR
International Journal of Information & Communication Technology Research

Volume 13- Number 3 – 2021 (1 -11)

Employing Machine Learning Approach in Cavity Resonator Sensors for Characterization of Lossy Dielectrics

Kianoosh Kazemi
Department of Electrical Engineering
Amirkabir University of Technology
Tehran, Iran
kazemikianoosh@gmail.com

Gholamreza Moradi*
Department of Electrical Engineering
Amirkabir University of Technology
Tehran, Iran
ghmoradi@aut.ac.ir

Received: 2 March 2021 - Accepted: 9 May 2021

Abstract—**This work presents a novel microwave sensor that is specially designed for the retrieval of complex permittivity. The proposed sensor is designed to operate in the C band (4.54 GHz). By implementing a novel feeding structure, the proposed SIW cavity design improves the coupling and achieves a better quality factor. Several techniques are used to enhance sensitivity, including a Photonic Band Gap (PBG), corner cut, and slow-wave vias. These techniques increase the interaction between the material under test and the electric field. By utilizing slow-wave vias, 35% size reduction is achieved. Achieving simultaneous miniaturization and sensitivity enhancement in this study introduces a new possibility and application for sensor design. The values of complex permittivities are extracted from scattering parameters obtained from simulation of the structure in CST Microwave Studio (MWS) using a machine learning approaches. Our sensor has 0.8% sensitivity, which is better than that of other sensors. Moreover, the maximum error rate in our method is lower than other existing methods. This ratio for the proposed method is 2.31% while for curve fitting and analytical solutions are 26% and 16%, respectively.**

Keywords: Complex Permittivity; Machine Learning (ML); Photonic Band Gap; Slow-Wave; Substrate Integrated Waveguide (SIW).

Article type: Research Article

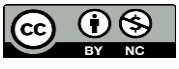

I. INTRODUCTION

Material characterization is crucial in various areas, including industry, agriculture, health care, and military applications. Permittivity and permeability are the main electromagnetic characteristics of materials. The RF and microwave characterization technics are amongst the methods providing accurate and noninvasive results [1]. These methods have been evolved and combined with other technologies and categorized in different methods such as transmission-line techniques, coaxial probes, free-space propagation methods, and cavity resonator technics [2], [3]. These methods are based on measuring the scattering

* Corresponding Author

parameters in the presence and absence of material under test (MUT). The main drawbacks in the techniques mentioned above, except for cavity resonators, are physical profile and sensitivity. However, cavity resonators provide high accuracy and less sensitivity to noises during measurements [4], [5]. Traditionally, in resonator-based techniques, the main component is metal waveguides. However, as a result of big size, heavy-weight, and inability to be integrated with other planar structures, the metal waveguide is being replaced with its counterpart known as the substrate integrated waveguide (SIW) [6]. Recently, SIW based structures are being investigated for various applications, which enable efficient design of SIW based cavities and filters at any desired frequency with low radiation and reflection losses as compared to the microstrip resonators [7].

In resonator-based techniques, cavity perturbation is highly popular for extracting electromagnetic characteristics of materials in the microwave frequency range. In contrast, this method suffers from different assumptions that deteriorate accuracy. In recent years, a few of these limitations are relaxed, which in turn improved the sensitivity remarkably [8], [9]. In addition to analytical solutions, the curve fitting methods are also established to obtain a mathematical relationship between the resonant frequency and permittivity [10], [11]. Sometimes, however, the relationship between frequency resonant and complex permittivity becomes complicated and impedes an analytical solution's derivation. In this regard, machine learning approaches are the best solutions for identifying the materials based on collected data [12]–[14]. Artificial neural networks (ANNs) and support vector machines (SVM) are suitable for reconstructing complex permittivity according to the measured values.

Cavity resonators are usually immersed in a large volume of liquid specimens [14], or their sample holders are filled with samples [15]. The interaction between the liquid and the electric fields is gained, and the scattering parameter reflects this interaction. Subsequently, by using scattering parameters, the liquid dielectric properties are calculated. Such methods, however, suffer from low sensitivity, and a considerable number of specimens is required.

In this work, a novel SIW sensor is designed and miniaturized by 35%. The sensor is equipped with photonic band gap (PBG) and internal via to reach the sensitivity of 0.80. Also, the proposed sensor's quality factor is enhanced remarkedly by using the novel tapering feed line. It is worth mentioning that unlike the other works [4], [5], [8], which are restricted to the cavity perturbation method which suffers from many limitations and assumptions, in this paper, a machine learning approach is adopted to extract the permittivity of the materials. Unlike other works [12], [14], which used resonance frequency shift as the input, this work is mainly based on morphology analysis of the scattering parameter. A set of features, including five features, is collected as the input data, and the relative permittivity and loss tangent are considered the output. Also, the proposed sensor has the potential to work under the condition where a small amount of sample is available and takes this advantage over its counterpart. In summary, the major contributions of the paper are as follows:

- Proposing a novel SIW sensor with a corner cut, PBG, and slow-wave (SW) vias which is miniaturized by 35%.
- Proposing a neural networks-based approach for retrieving the complex permittivity.
- Assessing the proposed method with other existing methods.
- Evaluating the proposed sensor in terms of sensitivity compared to other works.

The rest of the manuscript is organized as follows. The related work of this research is outlined in Section II. Section III is devoted to the cavity sensor design, including the geometry of the sensor and its simulation results. Section IV illustrates the sensor design procedure and parametric studies via simulation modeling for the return loss. Section V describes the development of the proposed method in detail. Section VI, contains the results and a general comparison between this work and recently published works. The final section summarizes the main conclusions of this work.

II. Permittivity Analysis Approaches

Several permittivity measurement methods with different complexities have been developed in the last decades. Most permittivity measurement methods contain three main algorithms: i.e., A) Analytical solutions, B) Curve fitting, and C) Machine learning-based methods.

A. Analytical Solutions

Cavity perturbation is one of the well-known approaches for retrieving the material properties (i.e., permittivity and permeability) in cavity resonator-based sensors. In cavity perturbation, the variation in resonant frequency and quality factor of the cavity is used as a signal for calculating the complex permittivity of materials placed at the maximum electric field position. The formula for the SIW cavity is as follows [16]:

$$\varepsilon'_r = 1 + \frac{2}{C}\left(\frac{f_o - f}{f}\right) \quad (1)$$

$$\varepsilon''_r = \frac{1}{C}\left(\frac{1}{Q} - \frac{1}{V_0}\right) \quad (2)$$

$$C = 4\frac{V_s}{V_c} \quad (3)$$

where f_0, f, Q_0, and Q show the resonant frequency and quality factor of an empty and filled cavity, respectively. In addition, C represents the shape factor coefficient while V_s and V_c are the sample size and the cavity size, respectively. These equations are based on three assumptions which are given as follows [17]:

Assumptions 1: The cavity walls are perfect electric conductor.

Assumptions 2: The electric and magnetic fields are constant throughout the sample volume.

Assumptions 3: Outside the test specimen, the cavity fields remain unchanged.

However, in practice, neglecting these assumptions would decrease the accuracy of the method substantially. In this regard, A.K. Jha *et al.* [9] have addressed the mentioned problems by proposing a new approach. They have relaxed the first assumption by utilizing a proper calibration during the measurements. In addition, the second assumption is relaxed by proposing a numerical optimization technique. The optimization approach tried to minimize the error between the measured and the theoretically (i.e., CST) calculated transmission loss (S_{21}) by using the interior-reflective Newton method. Moreover, the non-uniform variation of the electric field throughout the test sample was also taken into account, and as a result of the third assumption has been addressed as well.

The prevalence of planar technology has led to decreasing usage of metal waveguides for sensors as SIWs are more popular. SIWs combine the advantages of planar technology, and conventional waveguides [18]. Consequently, cavity perturbation expressions are error-prone when the sensor structure is based on SIW. This is originated from the quality factor difference between metal cavities and SIWs. In other words, the quality factor in metal cavities is as high as 5000, while in SIWs, the quality factor rarely reaches 1000. Therefore, Tiwari *et al.* [8] proposed new expressions for complex permittivity in SIW-based structures by considering the low-quality factor which is given as follows [8]:

$$\varepsilon'_r = \varepsilon'_s\left[1+\frac{2}{C_m}\left(\frac{f_o - f + k(k_0 f_0 - kf)}{f(1+k^2)}\right)\right] \quad (4)$$

$$\varepsilon''_r = \frac{1}{\varepsilon'_s}\left[\frac{2(\varepsilon'_s)^2}{C_m}\frac{f_o(k-k_o)}{f(1+k^2)} + \varepsilon'_r\varepsilon''_s\right] \quad (5)$$

where $C_m$is the modified shape factor, $k = (1 - |S_{21}|)/2Q$, and $k_0 = (1 - |S_{21}|)/2Q_0$.

However, analytical solutions are still insufficient when the test sample is not symmetrical on all axis. Also, this approach needs sample preparation before the measurement.

B. Curve Fitting

In addition, curve fitting techniques are developed for material characterization. These methods are mainly based on a mathematical relationship between the sensor's resonant frequency and the relative permittivity. In [19], a quad-band planar sensor was proposed based on complementary split ring resonators (CSRRs). In this study, the permittivity of dispersive materials was measured due to the multi-band nature of the sensor. Moreover, a curve fitting tool was used to establish a mathematical relationship between the inverse square of resonant frequency and the relative permittivity. In [20], two planar sensors based on split ring resonator (SRR) configuration are proposed. In this work, an inter-digital-based SRR and a meandered line SRR were designed for permittivity and permeability measurement. Following that, a mathematical model was established between resonance frequency shift and relative permittivity variation based on the minimum chi-square value. However, when the relation between the complex permittivity and resonance frequency becomes more intricate, the mathematical solution fails to determine the permittivity precisely.

C. Neural Network-Based Methods

ANNs are inspired by the human brain and imitate how biological neurons interact with one another, comprising an input layer, hidden layers, and an output layer [21]. Neural networks algorithms have been recently used in various microwave and mm-wave applications. Sun *et al.* [22], designed a planar symmetrical sensor combined of inter-digital capacitors and CSRRs. Moreover, they developed a back-propagation ANN for reconstructing the complex permittivity. The network was trained with training data, including resonance frequency and the transmission coefficient magnitude (i.e., $|S_{21}|$), generated from CST software. In [13], an array of CSRR, resonating in 5 various frequencies, was proposed. The proposed sensor operates in a wide frequency range from 1 to 10 GHz. In addition, they combined the result of 3 MUTs with different array combinations. Then, a decision-tree-based SVM was used for the classification of materials. Yang *et al.* [12] presented a SIW sensor, equipped with CSRR for improving the sensitivity, for characterizing the liquids. The sensor operated at 2.45 GHz. In addition, the permittivity of MUTs was determined using a neural network based on the parameters of actual experimental scattering.

III. Sensor Design

The detailed geometry of the proposed SIW structure is illustrated in Figs. 1 and 2. The microwave sensor is designed on a double-layer substrate of Rogers 4003 with permittivity and loss tangent of ε_r= 3.55 and tanδ= 0.0027, respectively, and a thickness of 1.6 mm. The selection of SIW structure is based on its low cost, easy fabrication, low radiation features, and more importantly, the capability of integration with other planar circuits. The resonant frequency in SIW is determined by effective width and length, as shown in the following equations [23]:

$$f_{mn0} = \frac{1}{2\pi\sqrt{\varepsilon\mu}}\sqrt{\left(\frac{m}{a_{\text{eff}}}\right)^2 + \left(\frac{n}{b_{\text{eff}}}\right)^2} \quad (6)$$

where the m and n are the mode indices, ε and μ represent the permittivity and permeability of materials, respectively, and a_{eff} and b_{eff} are the effective length and width calculated according to the (7) and (8) [14]:

$$a_{\text{eff}} = a_{\text{SIW}} - \frac{d^2}{0.95p} \quad (7)$$

$$b_{\text{eff}} = b_{\text{SIW}} - \frac{d^2}{0.95p} \quad (8)$$

where d and p are the diameter of the vias and the spacing between the vias, respectively. a_{eff} and b_{eff} are respectively the physical width and length of the SIW structure.

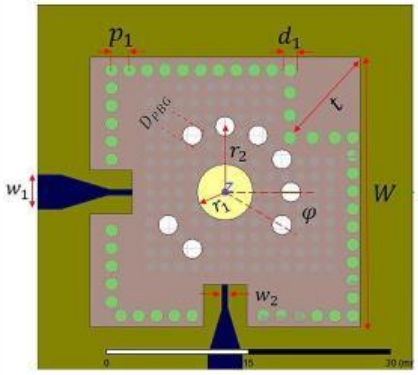

Fig 1. Configuration of sensor design.

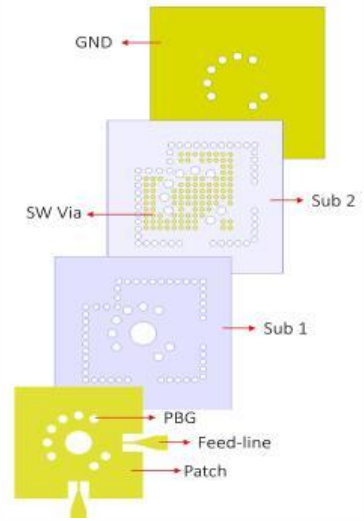

Fig 2. 3-D Configuration of sensor design.

where d and p are the diameter of the vias and the spacing between the vias, respectively. a_{eff} and b_{eff} are respectively the physical width and length of the SIW structure.

The sensor architecture is developed through several steps. First, a perturbation by some square corner cut is added to the structure. An array of PBG holes is then added to the sensor design to increase the concentration of electric field through wave encapsulation. In the next step, several rows of metalized vias are embedded in the lower substrate layer to reduce the sensor's size. Finally, by optimizing the diameter of MUT, the maximum amount of sensitivity is achieved.

The dimensions of the proposed structure are W = 26 mm, t = 4.5 mm, w_1= 3.65 mm, w_2= 0.6 mm p_1= 2.4 mm, d_1= 1.4 mm, r_1= 3 mm, r_2= 7 mm and these values are optimized to achieve the minimum insertion loss (S_{11}). The feedline of the sensor is a 50 Ω microstrip, which is matched to the structure using tapered microstrip to SIW transition [24]. This step is done to achieve a higher quality factor and to excite the cavity in undercoupled mode, which is suitable for permittivity extraction. The PBG array with the diameter D_{PBG}= 2 mm is arranged around the MUT with a radius of 5.25 mm, and an angle between two adjacent PBGs is set at 30°. The diameter of the internal metalized vias is 1 mm and the focal distance between two vias is fixed at 1.2 mm.

CST Microwave Studio software was used for simulation, and the return loss (at 3-8 GHz) is calculated for the sensor. The model is also simulated in HFSS frequency domain solvers to verify the obtained results (see Fig. 3). As shown in Fig. 3, both software's calculated reflection coefficient is almost the same, and there is a slight difference in resonance frequency, which is due to the difference in the solving method of HFSS and CST.

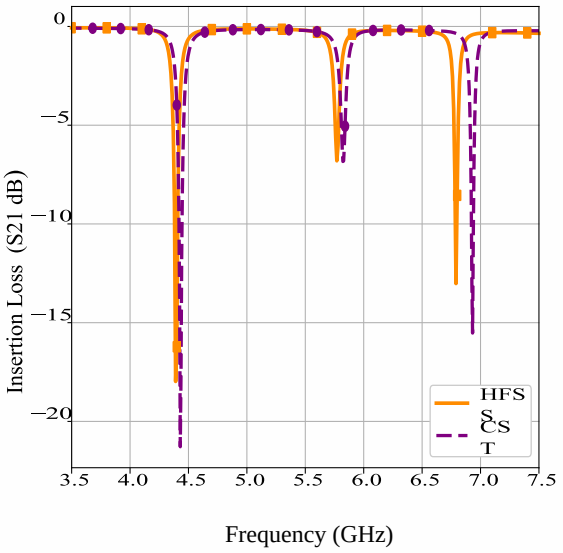

Fig 3. Simulation results (S11) based on CST and HFSS of the final proposed design.

IV. Simulation Result and Parametric Studies for Return Loss

Simulation and investigations are carried out using HFSS software. In the first step, the effect of adding SW via is studied, and based on this effect, the total size of the sensor is reduced. The sensor then is investigated under the presence and absence of PBG holes, and the diameter and location of these PBGs are parametrically studied for the highest sensitivity. Following this step, the corner of the cavity is perturbed by creating a square cut, and it is shown that this technique enhances the concentration of the electric field in the center of the sensor. Finally, the diameter of the MUT is varied to achieve the highest sensitivity.

Herein, in order to clarify that the proposed sensor exhibits a higher frequency shift compared with those introduced in [5], [12], [23], the frequency shift corresponding to gradual increase of the relative permittivity (ε_r) is plotted in Fig. 4. It can be seen that for each relative permittivity of the MUT, the frequency shift is higher in comparison with those given in [12], [23]. While this trend for [5] is exceeded for the MUT's relative permittivity from 1 to 10, and the frequency shift for the proposed sensor begins to be higher, the MUT's relative permittivity is higher than 10. Besides, the advantages of utilizing different

techniques are illustrated in Fig. 4. As shown in this figure, after using each method, the frequency shift is studied and plotted and shows the benefit of these methods.

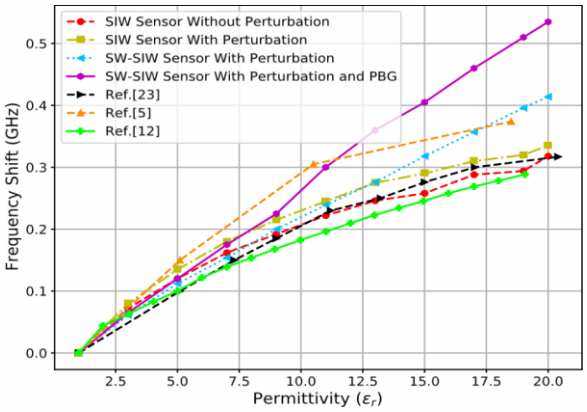

Fig 4. Simulated sensitivity of the frequency shift of the proposed sensor and that of the earlier works.

To achieve higher sensitivity, thus higher perturbation, the MUT should be placed at the region where the electric field concentration is high, which in this study is at the center of the cavity. Thus, by displacing the corner vias as a corner cut, the intensity of the electric field in the corner is squeezed into the center, and as a consequence, the higher electric field intensity is achieved in the center, where the MUT is located. This effect is clearly shown in Fig. 4. As we can see in this figure, by changing the dielectric constant of the sample from 1 to 20, the corresponding frequency shift for the sensor in the absence of square-cut perturbation is 318 MHz. However, after perturbing the sensor architecture with square-cut, the frequency shift reaches 335 MHz, meaning the sensitivity was improved by 5.34% in comparison with the former design.

Besides, a parametric study is conducted on the value of the perturbation size. The frequency shift for different materials is calculated for two perturbation cases, which by adjusting the t=8.37 mm, a higher sensitivity is achieved (see Fig. 5a). The reflection coefficient of the cavity is depicted in Fig. 5b. As shown in this figure, by increasing the t, the resonance frequency shifts to the higher frequency, and a better matching could be achieved.

A. Study of reflection coefficient for sensor design in presence and absence of SW vias

In this section the effect of adding slow-wave vias is studied in details. This technique is based on a double-layer substrate technology, where several rows of metalized via are inserted in the lower substrate and these slow-wave vias show a high slow-wave effect in the sensor leading to a reduction of the total size of the architecture. To exhibit this effect, a comparison is made on the sensor dimensions. Before adding the SW vias, the transversal and longitudinal length of the patch (W) was 40 mm and the 1st, 2nd, and 3rd resonance frequencies were 3.84 GHz, 5.67 GHz, and 6.09 GHz, respectively (see Fig. 6). After adding the internal vias, while the cavity dimension remains the same, the sensor resonates at 3.16 GHz, 4.69 GHz, and 5.11 GHz.

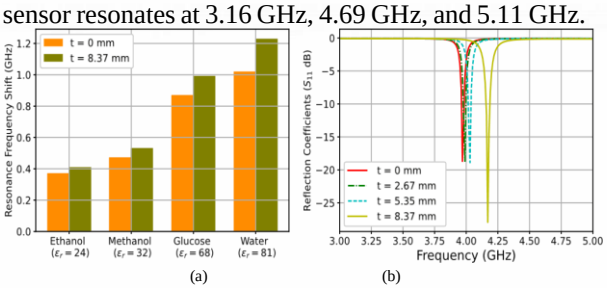

Fig 5. Example (a) Frequency shift in presence and absence of perturbation (b) Reflection coefficient for different values of perturbation size t.

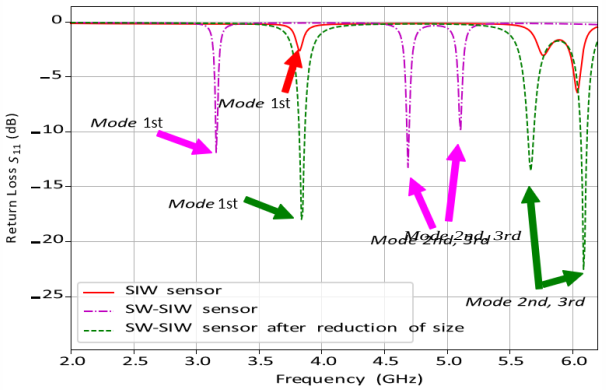

Fig 6. Frequency resonance of the structure before and after adding the SW vias.

To reach the same resonance frequency as the first step, in the final stage, the transversal and longitudinal length of the patch were reduced to 26 mm, in which the dimension is scaled down by 35%. Also, we can take another advantage of the slow-wave effect, separating electric and magnetic fields [25]. Based on this effect, the electric field's physical concentration increases in the upper substrate, where the MUT is located. Thus, the capacitive effect will rise in the upper substrate, and as a consequence, the sensitivity increases, as shown in Fig. 4. On the contrary, the magnetic fields remain unchanged in the whole volume of the sensor. To compare the sensitivity of the sensor with that of the previous section, as shown in Fig. 4, two cases are studied. In the first case, the sample place is empty, meaning that it is air, and in the second case, the sample place is filled with a sample (ε_r=20), and the frequency shift is calculated. This frequency shift was 414 MHz, which shows the sensitivity is increased by 23.58% compared with that of the sensor having a square corner cut.

B. Return loss studies with and without PBG

So far, the sensor is studied while it is equipped with SW vias and corner cut perturbation. In this section, the sensor's performance is studied when the PBG holes are added to the architecture of the design. By adding PBG holes, the cavity's reflection coefficient is slightly shifted (around 170 MHz) because of the PBG holes in the structure. In contrast, the magnitude of the reflection coefficient has changed negligibly. This frequency shift is mainly because of the substrate permittivity reduction and, consequently,

the resonance frequency shifts to a higher frequency. The parametric study, pervformed over the PBG holes location and diameter, is depicted in Fig. 7. As shown in Fig. 7, the main focus of this study is on the radius of the PBG and the repetition angle, and by considering the $repetition\ angle = 30°$ and the $distance\ from\ center = 5.25\ mm$, the maximum sensitivity can be achieved. Next, we impose the previous scenario, and the sensitivity of the architecture is compared with that of before and after adding PBG. The frequency shift for structure with PBG is 535 MHz, which is improved by 29.2% compared to the sensor in the absence of PBG.

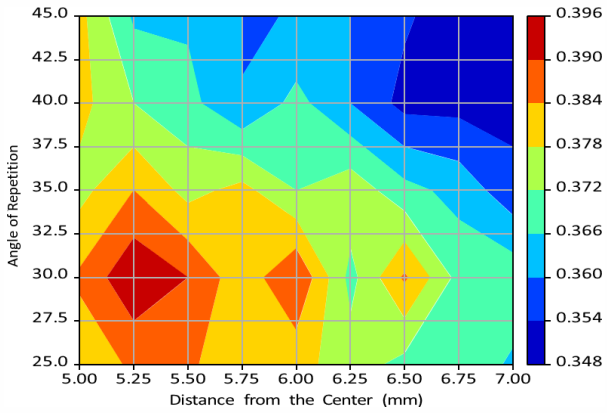

Fig 7. Frequency shift with respect to the PBG dimension and repetition angle.of a figure caption. *(figure caption)*

C. C. Study on the MUT's diameter for maximum sensitivity

The study of the sample's diameter is an indispensable step in achieving maximum sensitivity. In this regard, the sample diameter, as shown in Fig. 8a, is varied, and the corresponding resonance frequency is plotted for the different permittivities of the sample. Obviously, by increasing the sample's diameter, the resonance frequency would be affected. In contrast, as the permittivity of the samples increased, the operating frequency shifts to a lower frequency. Moreover, by increasing the sample diameter, the difference between resonance frequency is increased, showing a higher sensitivity. Hence, 3 mm is chosen as the sample's diameter for further assessment, providing the maximum sensitivity. It is evident that the larger sample causes the larger capacitance, and the higher the capacitance is, the higher the frequency difference could be. Also, to realize better, by increasing the sample's diameter in the constant intervals, the resonance frequency is plotted in Fig. 8b.

D. Parametric study of the electric field

In this section, the electric field distribution in each step is compared with one another. As illustrated in Fig. 9a, the electric field concentration in the sensor's center, where the MUT is located, is $3.2 \times 10^{4}(V/m)$ in the simple structure. By adding a perturbation in the architecture, the electric field concentration increased to $3.5 \times 10^{4}(V/m)$ (Fig. 9b). Then, adding the internal vias in the lower part of the substrate, as mentioned before, would affect the distribution of the electric field to be concentrated in the upper part of the substrate, which electric field increases to $3.7 \times 10^{4}(V/m)$ (Fig. 9c). Finally, the PBG holes causes the wave to be trapped in the center reign, which is due to periodic structure of PBG. This issue creates a band-gap in the frequency range and the trapped wave stops propagating in the cavity. This phenomenon increases the electric field concentration in the structure to $44.5 \times 10^{4}(V/m)$, as depicted in Fig. 9d [26].

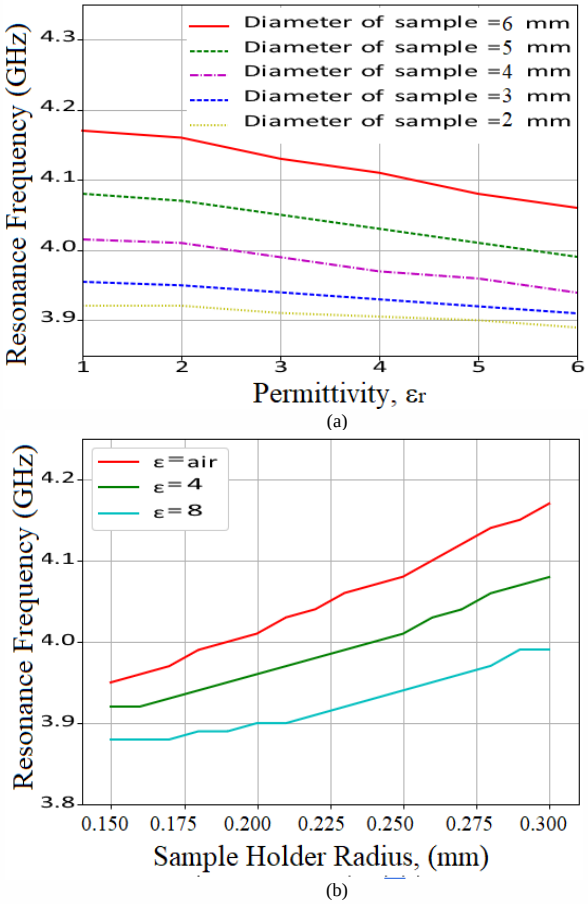

Fig 8. Resonant frequency changing associated with (a) Sample diameter for different permittivities (b) Permittivity for different sample diameters.

V. METHOD

A. A. Overview

In this section, we present a neural network-based method designed for complex permittivity prediction. The network is trained using the scattering parameter generated by CST. The method pipeline is shown in Fig. 10. As shown in this figure, at first, the model was simulated in CST with different materials, and their corresponding scattering parameters were collected. Then, different features were extracted from these scattering parameters. In the next step, a neural network was trained based on extracted features. In model usage phase, different MUTs were placed at the center of the sensor and their corresponding scattering parameters were collected. Following that, a set of features was extracted from the scattering parameter. Then by using the trained model, the complex permittivity of MUTs were predicted and compared with the original values.

B. Model training

In this phase, the procedure of permittivity prediction is discussed in detail. The proposed model was simulated with different samples with known dielectric properties and loss tangents.

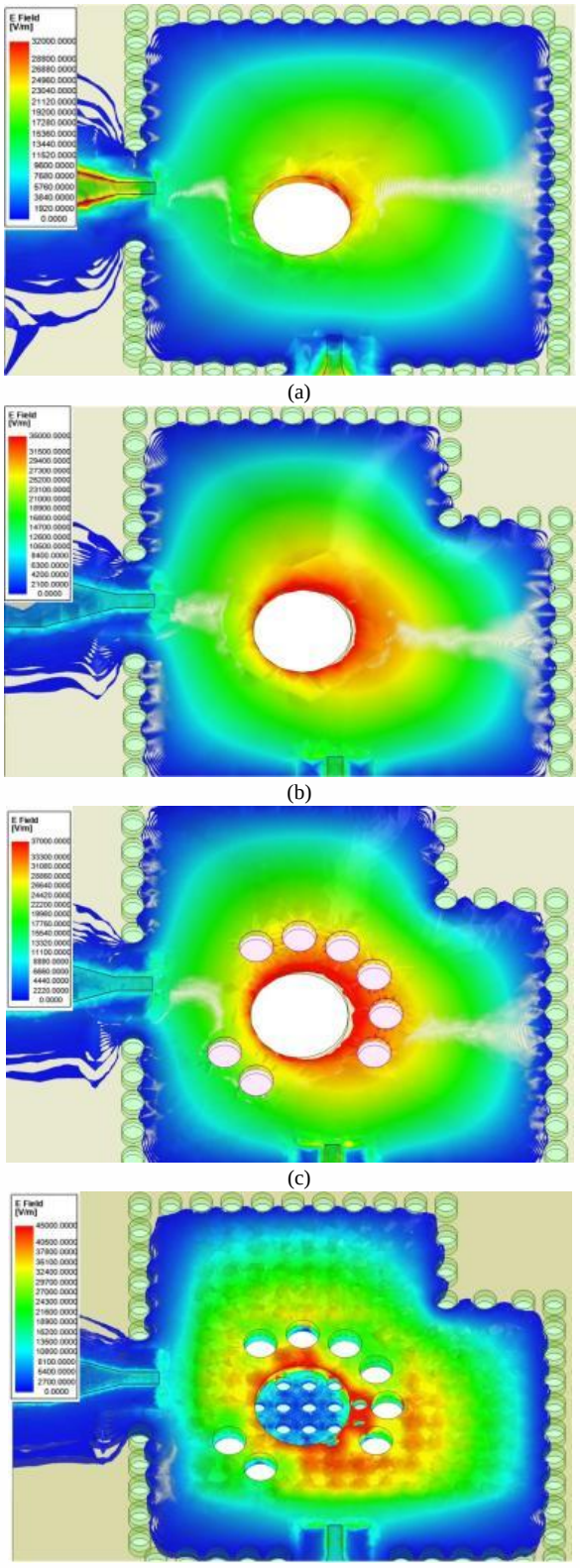

(a) (b) (c) (d)

Fig 9. Electric field distribution (a) Simple cavity (b) Simple cavity with a perturbation (c) Cavity with perturbation and PBG (d) Final design.

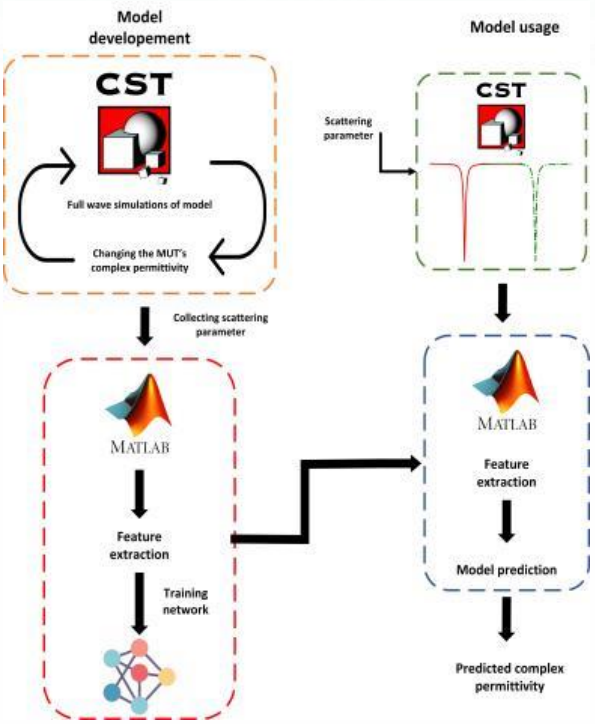

Fig 10. The proposed permittivity prediction method including data preparation, model architecture, and model prediction.

Fig. 11 presents the simulated reflection coefficient results of the SIW sensor for myriad permittivities (ε_r) and loss tangents ($\tan\delta$). As shown in Fig. 11, sharp notches are generated when the sample holder is filled with no sample (air ($\varepsilon r = 1, \tan\delta = 0$)). The maximum frequency shift is obtained when the permittivity varies from 1 to 65, which is 1550 MHz. The total number of simulations were 720 and the scattering parameter were collected from CST in the text files using MATLAB code.

Then, a set of different features, including the frequency resonance, the magnitude of scattering parameter, 3-dB bandwidth, quality factor, and the coupling coefficient [8], were extracted from the scattering parameter, a mapping relationship between these features and the complex permittivity. These parameters were first normalized so that all the features have the same range and avoid that higher weightage will be given to features with higher magnitude in the learning algorithm. The normalized data then fed to the feed-forward ANNs with two hidden layers, in which the first layer contains 11 hidden rectified linear unit (ReLU) nodes, comparing to other activation functions that have the ability to convergence faster, and the second one has two Sigmoid nodes, which these two nodes represent the relative permittivity and loss tangent. Also, the number of nodes is chosen 11 as the optimized number of nodes, resulting in higher accuracy. A higher number of nodes were also investigated in the training part; nonetheless, the test accuracy remained the same, but the training accuracy raised for higher nodes showing that the over-fitting occurred. The Levenberg-Marquardt algorithm is utilized to update the weight and consequently minimize the error between the input and target values [27]. Besides, the early stopping method was opted to

improve the generalization, and the early stopping is set when the validation error increases for six iterations and then the training was stopped. An artificial neural network is a group of neurons that are interconnected for processing the data based on mathematical models. The data, which was used for training the network, are collected from the simulation. To achieve the best performance, 80% of the data were used as the training data, 10% for cross-validation, and the remaining 10% for test. In Fig. 12, the regression analysis is depicted. Obviously, in this figure, the data are perfectly fitted to the approximated line to minimize the cost function. Moreover, the correlation coefficient (R) in all three stages (training, validation, and testing) is almost near unity, indicating the ANN's accuracy and validity. All the permittivity prediction procedures, including the learning and prediction steps, are carried out in MATLAB software.

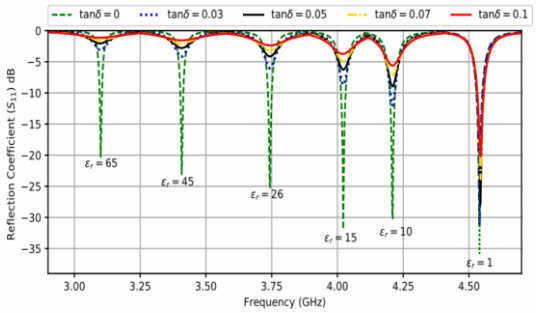

Fig 11. Frequency shift with respect to the PBG dimension and repetition angle. Simulated reflection coefficient of the designed sensor with respect to the permittivity (εr) and loss tangents (tanδ) of MUT.

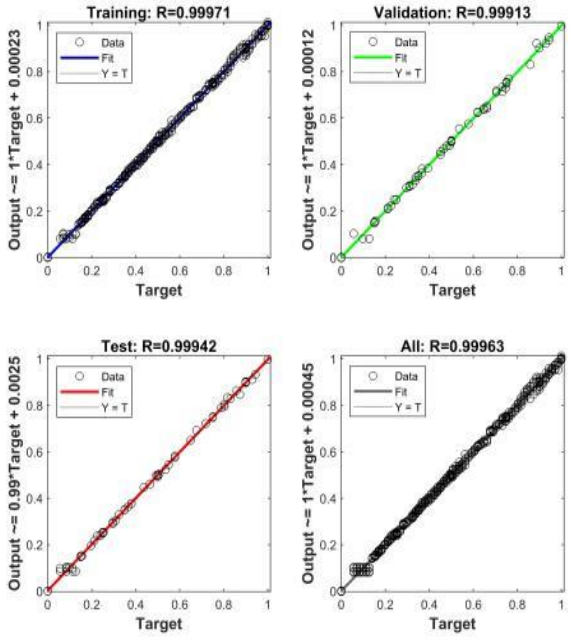

Fig 12. Regression plots by ANNs for the prediction of complex permittivity..

VI. Results and Discussions

To examine the accuracy of the network in the proposed sensor, different mixture of cyclohexane and water is used as a sample. In this study, the two liquids' complex permittivities are calculated from the first-order Debye model (9) [26].

$$\varepsilon^* = \varepsilon'(\omega) - j\varepsilon''(\omega) = \varepsilon_\infty - \frac{\varepsilon_\infty - \varepsilon_s}{1 + j\omega\tau} \quad (9)$$

where ε_∞ is the permittivity at the infinite frequency, ε_s is the static permittivity, ω is the angular frequency, τ is the relaxation time. In this study, the water is considered as the base liquid and the percentage of cyclohexane is varied [28]. Following that, the complex permittivity of the mixture is calculated using the two most widely used approximate mixing formula: Maxwell-Garnet (11) and Binary (10), respectively [10].

$$\varepsilon_{\text{eff}} = \varepsilon_1 f_1 + \varepsilon_2(1 - f_1) \quad (10)$$

$$\varepsilon_{\text{eff}} = \varepsilon_2 + \frac{3f_1\dfrac{(\varepsilon_1 - \varepsilon_2)}{\varepsilon_1 + 2\varepsilon_2}}{1 - f_1\dfrac{(\varepsilon_1 - \varepsilon_2)}{\varepsilon_1 + 2\varepsilon_2}} \quad (11)$$

where in (10) and (11), ε_{eff} is the effective permittivity of the mixture and f_1 is the volume fraction of the cyclohexane. The variation of the mixture relative permittivity (ε_r) and the loss tangent is illustrated in Figs. 13a, and 13b. As it can be seen from Figs. 13a, and 13b, the variation of the relative permittivity for different volume ratio starts from 73.74 and finally reaches 1.97. Also, the loss tangent varies between 0.21 and 0.004. Moreover, in this figure, the approximation obtained from these two formulae and also the results predicted from the ANNs are presented. As shown in these two figures, our results are closer to Maxwell-Garnet approximation.

First, we observe the variation of the mean square error (MSE) in 22 iterations of the ANNs model during training, cross-validation, and test information. The MSE is the square of the difference between predicted values and the input values (see (12)). In order to validate the ANNs, five-volume fractions of the cyclohexane-water mixture are calculated. We can see from Fig. 13 that the network fits the data effectively after five epochs [27].

$$\text{MSE} = \frac{1}{n}\sum_{i=1}^{n}\left(Y_i - \hat{Y}_i\right)^2 \quad (12)$$

In addition to the proposed method, we implement two exiting methods for permittivity detection. First, a curve fitting algorithm is used to establish the mathematical relationship between the resonant frequency and relative permittivity. In this regard, a fifth degree polynomial is used to plot this relationship.

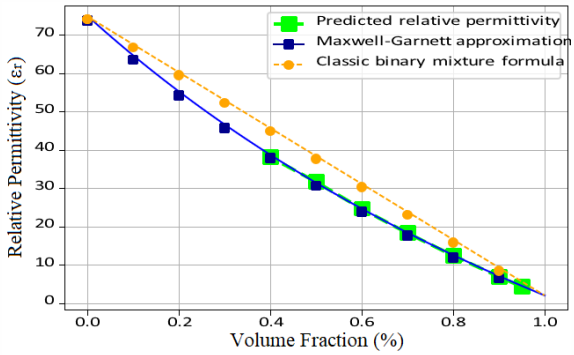

(a)

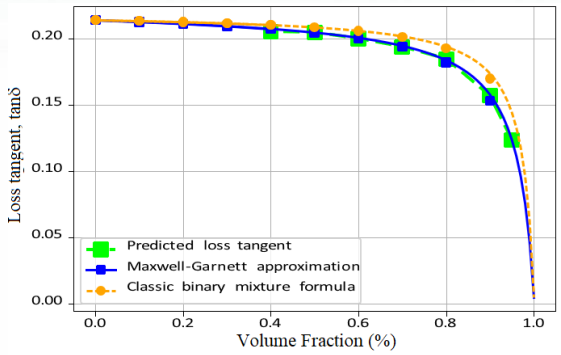

(b)

Fig 13. (a) The Relative permittivity (b) Loss tangent of the mixture of water and cyclohexane as a function of the volume.

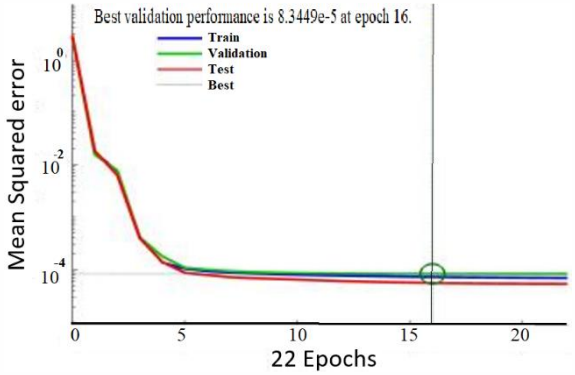

Fig 14. Example of a figure caption. *(figure caption)*

Fig. 15 illustrates the data points fitted using a polynomial curve fit and the derived equation for relative permittivity is given as follow:

$$\varepsilon_r = ax + bx^2 + cx^3 + dx^4 + ex^5 + f \quad (13)$$

where $a = -76187.087$, $b = 40860.727$, $c = -10928.72$, $d = 1456.4913$, $e = -77.35$, and $f = 56782.86$. Second, we use the method proposed by Tiwari *et al.* [8] as an analytical method. The equation for complex permittivity by [8] is already mentioned in section II.

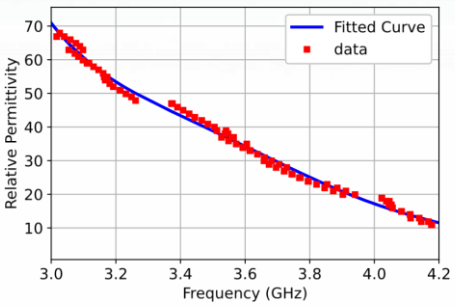

Fig 15. Fitted curve for extracting relative permittivity.*)*

Table I summarizes the simulated results for different volume fractions of the cyclohexane-water mixture. It is worth mentioning that by increasing the volume ratio of cyclohexane, the resonance frequency was decreased. This phenomenon can be explained by resonance frequency expression in cavities. According to equation 6, the higher the permittivity goes, the lower the resonance frequency will be. In addition, in our sensor, the increase in permittivity causes growth in both coupling factor and 3-dB bandwidth.

Moreover, a comparison between the performance of our method, curve fitting, and analytical solution for the different cyclohexane-water mixture is presented in Table II. As can be seen from Table II, the maximum relative permittivity and the loss tangent errors are 2.31%, and 0.55%, respectively, while these figures for curve fitting and analytical solution are 26%, 9.1%, and 16%, respectively. It should be noted that due to significant variation in insertion loss amplitude, using the curve fitting method for loss tangent, extraction was impossible.

A general comparison between this paper and other recently published work is performed in Table II to have a fair comparison. As shown in this table, the proposed sensor is far smaller than other similar sensors, and also, the sensitivity of this design exhibits a higher value, meaning that the sensor can easily discriminate very close permittivity values. Moreover, in terms of accuracy, our method obtained the higher value of accuracy (i.e. 0.80) while the other works sensitivity is below 0.7, i.e., 0.366 in [11], 0.7 in [12], and 0.53 in [29], respectively.

TABLE I. SIMULATED DATA FOR DIFFERENT MIXTURE VOLUME RATIOS

Volume fraction (%)	Simulated frequency (GHz)	Coupling factor	3-dB bandwidth (MHz)	Quality factor	Peak amplitude
95	4.40	0.877	101	43	-7.14
90	4.31	0.908	134	32	-9.87
80	4.15	0.932	198	20	-1.37
70	3.99	0.943	258	15	-1.67
60	3.81	0.950	315	12	-1.93

TABLE II. COMPARISON BETWEEN OUR METHOD AND OTHER EXISTING METHODS.

Volume fraction (%)	Theoretical complex Permittivity [27]	Predicted complex permittivity	Relative permittivity error (%)	Loss tangent error (%)	Curve Fitting	Relative permittivity error (%)	Analytical solution [8]	Relative permittivity error (%)	Loss tangent error (%)
95	4.48 -j0.55	4.37 -j0.53	2.31	0.55	5.52	26	4.23-j0.48	5.5	12.7
90	7.06- j1.109	6.97 -j1.094	1.33	0.07	8.53	22	7.22-j1.17	2.26	5.5
80	12.5 -j2.31	12.48 -j2.30	0.095	0.103	12.77	2.3	11.97-j2.7	4.2	16
70	18.33-j3.55	18.37 -j3.56	0.25	0.02	17.51	4.6	17.14-j3.6	6.5	2.2
60	24.59-j4.918	24.45 -j4.87	0.53	0.23	24.82	1.5	26.86-j5.1	9.1	3

TABLE III. COMPARISON OF RECENTLY PUBLISHED WORKS AND THIS WORK.

Ref.	Year	Sensitivity[a]	Operating frequency (GHz)	Physical size (mm)	Volume (μL)	Type
[11]	2018	0.366	2.188	55×50×5.625	226	Square SIW re-entrant cavity resonator
[12]	2017	0.7	2.45	85.09×50×5	150	SIW cavity resonator
[29]	2016	0.53	1.5	100×55×1.6	102	SIW cavity resonator
This work	2021	0.80	4.54	26×26×1.6	23	SIW cavity resonator

VII. CONCLUSIONS AND FUTURE WORK

Accurate complex permittivity determination is required to understand the electromagnetic behavior of materials in the microwave region. In the past decades, many methods have been proposed to provide accurate permittivity detection. These permittivity detection methods include analytical solutions and curve fitting. They are designed to establish a mathematical relationship between frequency variation and the changes in permittivity. However, when this mapping procedure becomes complicated, they fail to determine the permittivity precisely. This work designed a planar microwave sensor based on SIW architecture with high sensitivity to extract the complex permittivity. Simulating the model was conducted in a full-wave simulator, the CST, and verifying the model was done with the HFSS software. The sensor has been developed through multiple steps, and each step is discussed in detail. The proposed sensor outperformed in terms of sensitivity with other recently published works. The frequency sensitivity with respect to permittivity in our architecture was 0.80, while the other studies in the literature achieved a sensitivity lower than 0.70. Our algorithm for complex permittivity extraction was based on ANNs. The ANNs investigated in this study indicate a high level of reliability and accuracy based on the correlation coefficient of 0.99 in training, cross-validation, and test data. Our results indicate that the proposed complex permittivity detection method was successful in accuracy in a wide range of permittivity values. It can be derived from this study that the ANNs, which have been employed, is a fast and accurate tool for predicting the complex permittivity of materials.

The initial analysis shows encouraging results of the method's performances. However, our evaluation was restricted to five features extracted from the scattering parameter. The future direction of this study is to extract other different features such as phase information to address the lack of generalizability of the results.

Finally, the scattering parameters utilized in the training phase were noise-free. However, in practice, there is always a certain level of noise. In our future work, we intend to add arbitrary white Gaussian noise to the simulated scattering parameters.

REFERENCES

[1] S. Trabelsi and S. O. Nelson, "Microwave sensing of quality attributes of agricultural and food products," *IEEE Instrum. Meas. Mag.*, vol. 19, no. 1, pp. 36-41, Feb. 2016.

[2] Z. Akhter and M. J. Akhtar, "Free-space time domain position insensitive technique for simultaneous measurement of complex permittivity and thickness of lossy dielectric samples," *IEEE Trans. Instrum. Meas.*, vol. 65, no. 10, pp. 2394-2405, Oct. 2016.

[3] S. Subbaraj, V. Ramalingam, M. Kanagasabai E. Sundarsingh, Y. Selvam, and, S. Kingsley, "Electromagnetic nondestructive material characterization of dielectrics using EBG based planar transmission line sensor," *IEEE Sensor J.*, vol. 16, no. 19, pp. 7081-7087, Oct. 2016.

[4] Y. J. Cheng and X. L. Liu, "W-band characterizations of printed circuit board based on substrate integrated waveguide multi-resonator method," *IEEE Trans. Microw. Theory Techn.*, vol. 64, no. 2, pp. 599-606, Feb. 2016.

[5] J. Cai, Y. J. Zhou and X. M. Yang, "A metamaterials-loaded quarter mode SIW microfluidic sensor for microliter liquid characterization," *J. Electromagn. Wave*, vol. 33, no. 3, pp. 261-271, Nov. 2018.

[6] D. Deslandes and K. Wu, "Integrated microstrip and rectangular waveguide in planar form," *IEEE Microw. Wireless Compon. Lett.*, vol. 11, no. 2, pp. 68–70, Feb. 2001.

[7] H. B. Wang and Y. J. Cheng, "Broadband printed-circuit-board characterization using multimode substrate-integrated-waveguide resonator," *IEEE Trans. Microw. Theory Techn.*, vol. 65, no. 6, pp. 2145–2152, Jun. 2017.

[8] N. K. Tiwari, A. Jha and P. Varshney, "Generalized multimode SIW cavity-based sensor for retrieval of complex permittivity of materials," *IEEE Trans. Microw. Theory Techn.*, vol. 66, no. 6, pp. 3063-3072, Jun. 2018.

[9] A. K. Jha and M. J. Akhtar, "A generalized rectangular cavity approach for determination of complex permittivity of materials," *IEEE Trans. Instrum. Meas.*, vol. 63, no. 11, pp. 2632–2641, Nov. 2014.

[10] M. Saadat-Safa, V. Nayyeri, A. Ghadimi, M. Soleimani and O. M. Ramahi, "A pixelated microwave near-field sensor for precise characterization of dielectric materials," *Sci. Rep.*, vol. 9, no. 1, pp. 1-12, 2019.

[11] Z. Wei, J. Huang, J. Li, G. Xu, Z. Ju, X. Lio, and X. Ni., "A high-sensitivity microfluidic sensor based on a substrate integrated waveguide re-entrant cavity for complex permittivity measurement of liquids," *Sensors*, vol. 18, no. 11, pp. 4005, Nov. 2018.

[12] X. Yang, L. Xin, X. Jiao, P. Zhou, S. Wu, and K. Huang, "High-sensitivity structure for the measurement of complex permittivity based on SIW," *IET Sci. Meas. Technol.*, vol. 11, no. 5, pp. 532-537, 2017.

[13] L. Harrsion, M. Ravan, D. Tandel, K. Zhang, T. Patel and R. Amineh, "Material identification using a microwave sensor array and machine learning," *Electronics*, vol. 2, no. 8, pp. 288, Feb. 2020.

[14] C. Liu and F. Tong, "An SIW resonator sensor for liquid permittivity measurements at C band," *IEEE Microw. Wireless Compon. Lett.*, vol. 25, no. 11, pp. 751-753, Nov. 2015.

[15] E. Silavwe, N. Somjit and I. D. Robertson, "A microfluidic-integrated SIW lab-on-substrate sensor for microliter liquid characterization," *IEEE Sensors J.*, vol. 16, no. 21, pp. 7628-7635, Nov. 2016.

[16] A. K. Jha and M. J. Akhtar, "Design of multilayered epsilon-near-zero microwave planar sensor for testing of dispersive materials," IEEE Trans. Microw. Theory Techn., vol. 63, no. 8, pp. 2418-2426, Aug. 2015.

[17] R. F. Harrington, Time-Harmonic Electromagnetic Fields. New York, NY, USA: Wiley-Interscience, 2001, pp. 317–349.

[18] M. Bozzi, A. Georgiadis, and K. Wu, "Review of substrate-integrated waveguide circuits and antennas", IET Microw., Antennas Propag., vol. 5, no. 8, pp. 909-920, 2011.

[19] M. A. H. Ansari, A. K. Jha, Z. Akhter and M. J. Akhtar, ”Multi-band RF planar sensor using complementary split ring resonator for testing of dielectric materials”, IEEE Sensors J., Apr. 2018.
[20] K. T. M. Shafi, A. K. Jha and M. J. Akhtar, ”Improved planar resonant RF sensor for retrieval of permittivity and permeability of materials”, IEEE Sensors J., vol. 17, no. 17, pp. 5479-5486, Sep. 2017.
[21] C. C. Aggarwal, ”Neural Network and Deep Learning”, *Springer*, 2018.
[22] H. Sun, T. Tang, and G. Du Improved approach using symmetric microstrip sensor for accurate measurement of complex permittivity”, Int. J. RF Microw. Comput. Eng. 28.5, pp. e21258, 2018.
[23] Y. Seo, M. U. Memon and S. Lim, ”Microfluidic eighth-mode SubstrateIntegrated-Waveguide antenna for compact ethanol chemical sensor application,” *IEEE Trans. Antennas Propag.*, vol. 64, no. 7, pp. 3218-3222, Jul. 2016.
[24] D. Dslandes, ”Design equations for tapered microstrip-to-substrate integrated waveguide transitions *Proc. IEEE MTT-S Int. Microw. Symp. Digest (MTT)*, pp. 1-1, May. 2010.
[25] A. Niembro-Mart´ın, *V. Nasserddine, E. Pistono*, H. Issa, and P. Ferrari, ”Slow-wave substrate integrated waveguide,” *IEEE Trans. Microw. Theory Techn.*, vol. 62, no. 8, pp. 1625-1633, Aug. 2014.
[26] K. Kazemi, G. Moradi and A. Ghorbani, ”Employing higher order modes in broadband SIW sensor for permittivity measurement of medium loss materials,” *Int. J. Microw. Wireless. Technol.*, pp. 1-13, Oct. 2020.
[27] S. Huang, Z. Cao, H. Yang, Z. Shen and X. Deng, ”An electromagnetic parameter retrieval method based on deep learning,” *J. Appl. Phys.*, vol. 127, no. 22, p. 224902, Jun. 2020.
[28] (2019), *CST-Computer Simulation Technology* [Online], Available: https://www.cst.com.
[29] P. K. Varshney, N. K. Tiwari and M. J. Akhtar, ”SIW cavity based compact RF sensor for testing of dielectrics and composites,” *IEEE MTTS International Microwave and RF Conference (IMaRC)*, New Delhi, pp.
1-4, 2016.

Kianoosh Kazemi was born in Shiraz, in 1995. In 2017, he received his B.Sc. degree from Shiraz University in Electrical Engineering. In 2019, he obtained his M.Sc. degree from the Amirkabir University of Technology (Tehran Polytechnic), Tehran, Iran. In March 2021 he joined the Department of Computing at Aalto University as a researcher. He is currently a Ph.D. candidate at the University of Turku, working on Smart Health Monitoring Frameworks Based on the Internet of Things and Machine Learning Approaches.

Gholamreza Moradi received the Ph.D. degree in electrical engineering from Amirkabir University of Technology (Tehran Polytechnic), Tehran, Iran in 2002. His main research interests are Microwave Imaging, Numerical Electromagnetics, Antennas, Active Microwave MM-Wave and THz Systems. He is conducting some collaborative projects on 5G Antenna together with the University of Alberta and the University of Dresden. Dr. Moradi is currently an Associate Professor with the Department of Electrical Engineering, Amirkabir University of Technology. He has published over one hundred papers in the refereed journals and international conferences.